International Journal of Bioprinting

REVIEW ARTICLE

Up-to-date progress in bioprinting of bone tissue

Yang Wu[1,2]*, Ming Li[1], Hao Su[1], Huaying Chen[1], Yonggang Zhu[1]

[1]School of Mechanical Engineering and Automation, Harbin Institute of Technology, Shenzhen, China

[2]State Key Laboratory of Fluid Power and Mechatronic Systems, Zhejiang University, Hangzhou, China

(This article belongs to the *Special Issue: Composite/Multi-component Biomaterial Inks and Bioinks)*

Abstract

The major apparatuses used for three-dimensional (3D) bioprinting include extrusion-based, droplet-based, and laser-based bioprinting. Numerous studies have been proposed to fabricate bioactive 3D bone tissues using different bioprinting techniques. In addition to the development of bioinks and assessment of their printability for corresponding bioprinting processes, *in vitro* and *in vivo* success of the bioprinted constructs, such as their mechanical properties, cell viability, differentiation capability, immune responses, and osseointegration, have been explored. In this review, several major considerations, challenges, and potential strategies for bone bioprinting have been deliberated, including bioprinting apparatus, biomaterials, structure design of vascularized bone constructs, cell source, differentiation factors, mechanical properties and reinforcement, hypoxic environment, and dynamic culture. In addition, up-to-date progress in bone bioprinting is summarized in detail, which uncovers the immense potential of bioprinting in re-establishing the 3D dynamic microenvironment of the native bone. This review aims to assist the researchers to gain insights into the reconstruction of clinically relevant bone tissues with appropriate mechanical properties and precisely regulated biological behaviors.

Keywords: Bioprinting; Bone; Vascularization; Tissue engineering; Mechanical enhancement

***Corresponding author:**
Yang Wu
(wuyang2019@hit.edu.cn)

Citation: Wu Y, Li M, Su H, *et al*., 2023, Up-to-date progress in bioprinting of bone tissue. *Int J Bioprint*, 9(1): 628.
https://doi.org/10.18063/ijb.v9i1.628

Received: April 15, 2022

Accepted: July 20, 2022

Published Online: October 28, 2022

1. Bone: Anatomy and functions

Bone has several crucial functions in the musculoskeletal system, including protecting organs, producing blood cells, storing minerals, and mechanically supporting the human body[1]. According to their macrostructure, the bone can be categorized into cortical (or compact) bone or cancellous (or trabecular) bone. Up to 80% of total bone mass consists of cortical bone, which is dense and has low porosity, contributing to bone's mechanical strength[2]. Comparatively, the porous structure of trabecular bone results in tissue with a low compressive strength (e.g., one-tenth that of cortical bone)[2]. As a result of a large surface-to-volume ratio, the trabecular bone provides a structure that allows for good contact between bone and blood cells, which is essential for controlling hematopoiesis and homeostasis[3]. As an example, a long bone has three key regions, including a dense cylindrical shaft made of cortical bone (diaphysis) and two sections at the end made

of trabecular bone (metaphysis). Microscopically, bone lamella, which is composed of mineralized collagen fibers, exhibits a planar arrangement with a width of 3 – 7 μm[4]. In cortical bone, osteons (or Haversian systems) are formed by concentric layers of lamellae wrapped around a central canal. On the other hand, the arrangement of mineral platelets in the trabecular bone is different, in which the mineral platelets are aligned with the collagen fibers[2].

Furthermore, lamellae, which are considered the basic building blocks of bone, contain mineralized collagen fibrils (~100 nm in diameter). Collagen type I (COL-I) is the primary organic component of the matrix, which is secreted by osteoblasts followed by self-assembling. Apatite crystals distribute discretely along the collagen fibrils. The lamellae and collagen fibers of bone are organized in a way that prevents crack propagation and increases bone toughness[5]. As for the composition of bone, hydroxyapatite (HAp, 60%) and collagen-I (20%) are the major substances. Besides, there are several types of impurities in bone, including sodium (Na^+), magnesium (Mg^{2+}), and potassium (K^+), as well as proteins, such as osteocalcin (OCN), osteonectin, and sialoprotein[6]. Osteoblasts, osteocytes, osteoclasts, and bone lining cells are the four types of cellular components of bone that are embedded in the extracellular matrix (ECM). Osteoblasts, the bone-forming cells, consist of 4 – 6% of the total number of bone cells. ECM is synthesized by osteoblasts in a two-step process involving the deposition of organic matrix followed by mineralization[7]. During the calcification process, osteoblasts transform into osteocytes, which distribute in the ECM and act as stress sensors in the bone. In some cases, osteoblasts stay on the top of new bone and protect the bone underneath, hence the term lining cells. A bone osteoclast is a very large, multinucleate cell that absorbs bone matrix, in which function is critical in the maintenance, repair, and remodeling of bone.

Bone plays an essential role in providing the body with mechanical support. Calcium phosphate provides mechanical durability and high resistance to compression of bone, whereas collagen is responsible for bone's elasticity and resistance to tension and stretching. Young's modulus is approximately GPa for native bone, and tensile and compressive strengths are approximately MPa, which are determined by the location of the bone in the body or by the specific location within the bone. Compared with cancellous bone, cortical bone exhibits much higher Young's modulus (7 – 30 GPa vs. 50 – 500 MPa), tensile strength (50 – 150 MPa vs. 1.2 – 20 MPa), compressive strength (167 – 193 MPa vs. 1.9 – 10 MPa), and strain to failure (1 – 3% vs. 5 – 7%) in the longitudinal direction[8,9].

2. Consideration of bioprinting a bone

The conventional tissue engineering strategy is to seed cells onto scaffolds, which can then direct cell proliferation and differentiation into three-dimensional (3D) functioning tissues and organs. Although significant success has been achieved in the past decades both in research and clinical applications[10], it is obvious that complex 3D tissues require more precise multicellular structures, which cannot be fulfilled by traditional methods. Bioprinting offers a controllable fabrication process, which allows precise spatial placement of various biomaterials and/or cell types simultaneously mimicking the target natural tissue or organ[11]. Complementing the existing review articles about bioprinting and its applications[12-14], this review focuses on 3D bioprinting of bone, which is rapidly advancing in the field of regenerative medicine. This article discusses the up-to-date progress in 3D bioprinting technologies for bone reconstruction by integrating knowledge from *in vitro* and *in vivo* studies. Bioprinting approaches and other major considerations are carefully evaluated, such as bioprinting apparatus, biomaterials, bone vascularization, cell source, differentiation factors, mechanical properties and reinforcement, hypoxic environment, and dynamic culture. This review outlines the latest advancement in bioprinting of bone and aims to assist the researchers to gain insights into the reconstruction of clinically relevant bone tissues with appropriate mechanical properties and precisely regulated biological behaviors.

In this review, studies based on conventional 3D printing, in which acellular scaffolds are fabricated followed by cell-seeding, are excluded from the study. Studies on the topic of bone bioprinting, in which cellular components are manipulated together with bioink deposition without subsequent manual cell-seeding process, are carefully selected and reviewed. From the viewpoint of the authors, the selected studies are innovative in certain aspects such as bioink preparation, bioprinting process, or construct design and represent the state-of-the-art progress in this field. When discussing about bone bioprinting, the following questions should be kept in mind (Figure 1):

(i) What printing processes and structure designs can facilitate micro-/macroscale vascularization of bioprinted bone?
(ii) What is the optimal bioink formula for derive the greatest benefits from natural and synthetic biomaterials?
(iii) What are the best combinations of cell types for bone bioprinting? When multiple cell types are loaded in the bioink, how do they interact and promote osteogenesis of stem cells and the formation of vasculature?

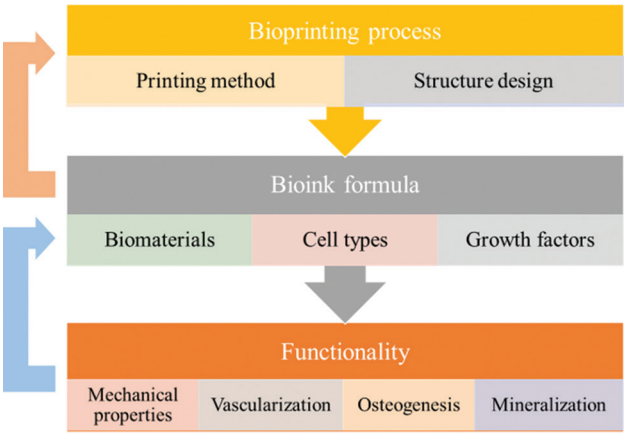

Figure 1. Design flow for bioprinting a bone construct.

(iv) Besides the well-acknowledged growth factors, are there other biologicsor supplements that can be incorporated in bioprinting and are they conducive to osteogenesis?
(v) What can be carried out to compensate for the weak mechanical properties of bioprinted bone resulting from the nature of cell-laden bioinks?
(vi) As bone cells are highly metabolically active, how does the hypoxic culture environment impact the maturation of bioprinted bone?
(vii) How do bone cells respond to mechanical stresses in the bioprinted constructs in terms of cell morphology, osteogenesis, and mineralization?

2.1. Bioprinting apparatus

The common bioprinting processes, including extrusion-based bioprinting (EBB), droplet-based bioprinting (DBB), and laser-based bioprinting (LBB), have been utilized for bone bioprinting, depending on the selective bioink formula. In EBB, the bioink is deposited from a syringe or nozzle onto a build platform based on a computer-aided design of the structure to be printed (Figure 2A). This is accomplished by laying down small cylindrical deposits of the material, either pneumatically, mechanically, or by solenoid-driven deposition. In general, bioprinted bone constructs are primarily fabricated by EBB due to its efficiency in printing large-scale constructs in 3D, and its flexibility to handle a variety of biomaterials to obtain sufficient mechanical strength. Meanwhile, in DBB, bioink with modulated fluid properties (e.g., surface tension and viscosity) is manipulated to form droplets and then constructed using gravity, atmospheric pressure, and fluid mechanics[15] (Figure 2B). The LBB process involves the use of a laser pulse directed through a mirror onto a layer of bioink. In LBB processes based on photopolymerization, an ultraviolet (UV) laser is used to cure hydrogels in a vat that is capable of photocrosslinking (Figure 2C). To build the final construct, this process is repeated several times in a layer-by-layer manner[16,17].

Aspiration-assisted bioprinting (AAB), which has recently been developed to manipulate cell spheroids, is a new bioprinting technique that capitalizes on the fact that spheroids can be formed from diverse cell types at high densities, lifted by employing negative air pressure, and bioprinted on a hydrogel[18] (Figure 2D). The above-mentioned bioprinting processes are sometimes integrated to obtain optimal mechanical and biological properties.

2.2. Selection of bioink

Different cellular responses have been observed when natural hydrogels are used for bone bioprinting. For bone bioprinting, alginate has always proven to be a popular biomaterial due to its biocompatibility, low cost, and ease of cross-linking by contact with calcium (Ca^{2+}) ions[19]. The low bioactivity of alginate poses a limitation to its use. As compared, the similarities between collagen and native bone make it an ideal material for bone bioprinting. It is, however, difficult to generate collagen hydrogels with high viscosity that have rapid gelation capabilities. Therefore, collagen was only used in a handful of bone bioprinting studies, usually in combination with other biomaterials. Since gelatin is derived from collagen, it is a more economical option and is used in conjunction with other biomaterials to form bioinks. The biological functions of bioprinted bone can also be regulated by other popular biomaterials, such as agarose, chitosan, and hyaluronic acid (HA)[20,21]. Aside from mixing several natural polymers with varying concentrations to tailor bioink properties, polymers can also be modified to have customized properties. For example, methacrylate hydrogels, which are natural components of the ECM modified by methacrylation, are widely used in the field of bioprinting[22]. As one of those hydrogels, gelatin methacrylate (GelMA) is becoming a popular biomaterial for 3D bioprinting[23,24], due to its biocompatibility as well as its ability to cross-link chemically with UV light under physiological conditions[25]. Another example of hydrogel is methacrylated HA (MeHA)[26], which has been combined with GelMA hydrogel for bone bioprinting[27].

These above-mentioned polymers can directly bioprint with cells; however, the application of cell-laden hydrogels in hard tissue regeneration has been restricted by their low mechanical properties[28,29]. Consequently, biomaterials such as ceramics, thermoplastics, or alloys that were traditionally used for the manufacture of bone scaffolds could be incorporated with hydrogels to boost the mechanical strength of the bioprinted bone[28,30-32]. There are multiple options for biomaterials that imitate the

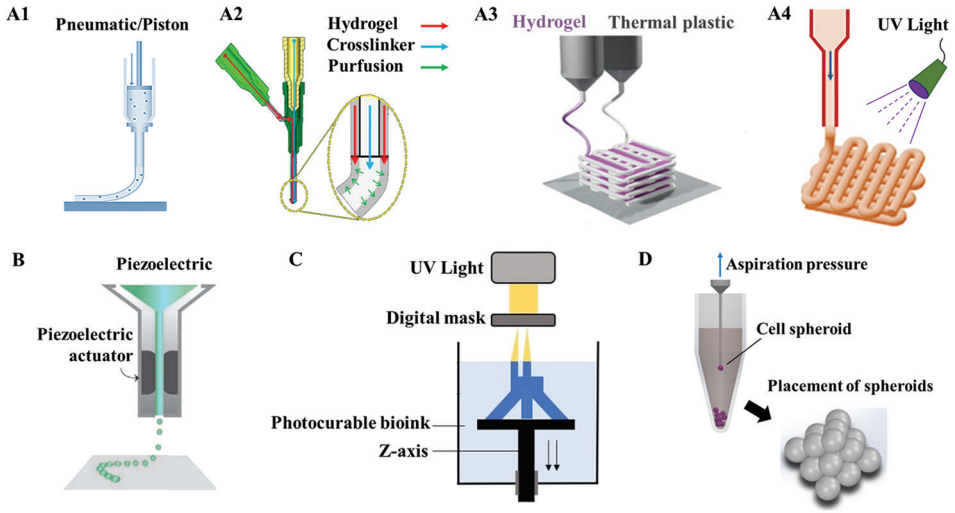

Figure 2. Bioprinting technologies for bone tissue. (A) Extrusion-based bioprinting with traditional pneumatic/piston extrusion (A1), coaxial nozzle for the printing of core-shell filaments (A2), dual-nozzle setup for bioprinting of multiple bioinks (A3), and post-printing polymerization for photocurable bioink, (B) droplet-based bioprinting, (C) laser-based bioprinting, and (D) aspiration-assisted bioprinting.

main components of bone, including HAp and tricalcium phosphate (TCP)[33-35], as well as polycaprolactone (PCL), polylactic acid (PLA), and polyether ether ketone, which are known for their great mechanical properties[36]. Furthermore, studies have been conducted with 45S5 Bioglass, polyP, and biosilica, which enhance the ability of cells to synthesize mineral deposits and induce the expression of alkaline phosphatase (ALP), bone morphogenetic protein 2 (BMP-2), and COL-I[37,38].

2.3. Vascularized bone structure

Considering that bone is a complex tissue with a hierarchically organized structure, biomimetic design becomes an essential consideration. Cells within the bone are encapsulated by the mineral matrix, which is surrounded by blood vessels[39-42]. It is widely recognized that interconnected pores are necessary for the growth of blood vessels. According to the general viewpoint of tissue engineering, a pore size of 5 microns is optimal for neovascularization, 5 – 15 microns for fibroblast ingrowth, 40 – 100 microns for osteoid ingrowth, and 100 – 400 microns for bone regeneration[43,44]. Other than the use of porous structures, a number of strategies have been developed to promote angiogenesis, including the use of angiogenic growth factors[45,46], dynamic culture[47], and coculture of endothelial cells (ECs) with mesenchymal stem cells (MSCs)[48-50].

A functional blood vessel system at the network level within the implant is required for the effective restoration of bone. It is expected that the endothelium and vessel wall are organized in a networked fashion. In this context, bioprinting is possible to remodel a hierarchically branched vascular network with anatomic similarity. In one case, a geometry consisting of two phases was envisioned, with HAp forming part of the shape (bone tissue) and alginate and gelatin filling the tubular structure (vascular structure)[51]. Moreover, Byambaa *et al.*[52] designed a pyramidal construct that included a perfusable vascular lumen and was functionalized with gradient concentrations of vascular endothelial growth factor (VEGF). Media perfusion for 5 days was performed to produce a hollow perusable main vessel. For example, Cui *et al.*[53] fabricated a biphasic structure using a dual bioprinting procedure that combined fused deposition modeling (FDM) and stereolithography (SLA). The honeycomb-pored units in the hard portion of the scaffold mimicked the osteon or Haversian system of bone, while the channels filled with GelMA hydrogel resembled the vascular system. Cell growth and expansion in the hydrogel were expected to render the formation of capillaries.

2.4. Cell source

Bone bioprinting has continued to use similar cell types that are popular in bone tissue engineering. A mouse osteoblast precursor cell line (MC3T3) has been proven to be highly feasible and physiologically relevant for bone bioprinting. Nevertheless, it is important to exercise caution when extrapolating these results to primary cells. In research pertaining to the bone, human osteosarcoma cell line (SaOS-2) that is derived from the primary osteosarcomas is commonly used as osteoblast-like cells[54]. The SaOS-2 cell line has several advantages, including the ability to propagate quickly and to differentiate in a manner similar to that of osteoblasts[55].

The multipotency of stem cells makes them a popular alternative to cell lines and primary bone cells. Numerous studies have been conducted on bone bioprinting using MSCs, such as bone MSCs (BMSCs) and human nasal turbinate-derived MSCs (hTMSCs)[56]. An intriguing finding is that MSCs can be obtained from induced pluripotent stem cells (iPSCs), which can overcome the problem of limited quantities of autologous MSCs[57]. Furthermore, adipose-derived stem cells (ADSCs) are plenty in the human body and are surgically accessible, which makes them another striking source for bioprinting[13]. To support therapeutic revascularization in bioprinted tissue, ECs[26,52,53], endothelial progenitor cells (EPCs)[58], or endothelial colony-forming cells (ECFCs)[59] have been cocultured with the above-mentioned cells[59-61].

2.5. Osteogenesis

In principle, bioprinted bone should promote and facilitate the proliferation and osteogenesis of stem cells and osteoprogenitor cells by the release of specific cytokines, such as transforming growth factor (TGF-β), interferons, and interleukins (IL)[62,63]. In addition, bioprinted bone should possess osteoinduction capabilities by depositing bone-related proteins (e.g., BMPs, insulin-like growth factors, and fibroblast growth factor [FGFs])[64-66]. Last but not least, the structure should provide a porous microenvironment for the differentiation of bone cells, facilitating the synthesis of minerals, and collagenous tissue[67].

Some of the above-mentioned studies have shown that stem cell differentiation is preserved in bioprinted bone, and their osteogenic differentiation can be modulated by utilizing the right printing process, biomaterials, design, and bioactive factors[68]. The addition of BMP-2 and TGF-β usually results in greater osteogenic differentiation[69,70]. As to bioink materials, an alginate-based hydrogel supports the viability of MSCs and retains their osteogenic capacity in bioprinted bone[71]. MeHA has also been demonstrated to trigger osteogenic differentiation of hBMSCs in bioprinted constructs without exogenous osteogenic factors[72]. The GelMA scaffold was also demonstrated to induce mineralization of MG63 osteoblasts and primary normal human osteoblasts (NHOst) without requiring any additional osteogenic factors[73]. In addition, the HAp plays an important role in the osteogenic differentiation of preosteoblast cells *in vitro*[74]. A surge of mineralization in SaOS-2 cell-embedded hydrogel was observed on overlaying polyP·Ca^{2+}-complex to the bioprinted alginate/gelatin hydrogel[75]. Furthermore, bone scaffolds that were composed of decellularized porcine bone had significantly enhanced osteogenic gene expression, without the use of an osteogenic medium[76]. Besides, the addition of biologically active ions like strontium (Sr^{2+}) has been reported to enhance bone formation[77,78]. In addition, as an alkaloid component extracted from Chinese traditional medicines such as astragalus and coptis, berberine also has an osteogenic effect and antibacterial properties[79]. Stiffer biomaterials also trigger higher MSC osteogenic differentiation as the mechanical properties of the biomaterial affect cellular activity[72]. Moreover, it has been reported that exogenous electrical stimulation can increase mineralization[80]. In short, using appropriate physical and chemical cues, the stem cell activities, particularly the osteogenesis, can be controlled and enhanced.

2.6. Mechanical enhancement

Constructs bioprinted using natural hydrogels have a low modulus of compression (<10 kPa)[74,81] and degrade rapidly, losing most of their structural integrity within a short-time[82]. Despite the design of delicate gradients with different concentrations of GelMA hydrogel, mechanical stability could not be maintained for more than 21 days in culture as a result of the degradation of GelMA[52]. Furthermore, the polyP·Ca^{2+} coated alginate/gelatin construct lost its mechanical stability after a 5-day culture[75]. Young's modulus (GPa) and tensile/compressive strength (MPa) of native bone are in some orders of magnitude higher than those of hydrogel-based bioinks. It is problematic to use hydrogel-only constructs in clinical applications, and thus, developing constructs with a high and retainable mechanical strength is urgent.

Blending mechanically strong particles within a hydrogel may provide some reinforcement to bioprinted constructs[51,74]. The compression modulus of cell-laden constructs containing alginate, polyvinyl alcohol (PVA), and HAp was 10.3 kPa, but this value dropped to 2.4 kPa after 14 days of culture[83]. An elastic modulus of 0.55 MPa has been measured for the bioprinted TCP-collagen constructs[84], which was less than the elastic modulus of trabecular bone (20 – 52 MPa)[85]. Using silk fibroin/ionic-doped β-TCP, a multilayer structure has been prepared, which provided slightly enhanced mechanical properties (static compression modulus of 0.66 MPa and dynamic mechanical properties of 2.17 – 3.19 MPa)[86]. Furthermore, nanozirconium dioxide powder was blended in PCL, and Young's modulus and compressive strength increased by ~0.4 and 0.5 times, respectively, as compared with the PCL-only scaffold[87]. In another case, bredigite was mixed with nanosheets of graphene oxide which was reduced by bovine serum albumin, and the addition of reduced graphene oxide enhanced the mechanical properties of scaffolds[88].

For significant reinforcement of the mechanical properties of bioprinted constructs, thermoplastics or

ceramic frames are usually 3D printed. The incorporation of thermoplastics not only enhances mechanical properties but also enables the creation of large-scale structures with very high fidelity and a high fiber resolution[89,90]. Using FDM of PLA to mimic the Haversian system of bone and SLA of GelMA to simulate the blood vessels, a scaffold was engineered that exhibited a similar mechanical strength to native bone, as indicated by the compressive modulus of ~0.38 GPa, while the elastic modulus of the vascular region was 10 – 30 kPa, offering an appropriate microenvironment for cell encapsulation[53]. Using PCL or PCL/TCP structures as support for cell-laden hydrogels, a compressive modulus of ~30 – 45 MPa was obtained using various PCL: TCP ratios[91]. In contrast to printing hydrogel and supporting frame separately, core/shell scaffolds were constructed, consisting of calcium-deficient hydroxyapatite (CDHA) core and cellular-laden alginate (shell)[92]. The integration of the CDHA core resulted in a significantly higher compressive modulus (7 MPa) than alginate-only scaffolds and preserved the structural integrity *in vitro* for 35 days.

2.7. Hypoxic culture

Hyperoxia is another factor that plays a significant role in bone development through the hypoxia-induced transcription factors (HIF), although there is debate about the impact of hypoxia on bone regeneration[93]. Studies have indicated that hypoxia enhances the osteogenesis of BMSCs[94-96], whereas others have suggested that hypoxia inhibits the growth and bone-forming ability of osteoblasts, such as the differentiation of MSCs into osteoblasts[97,98]. Hypoxia and HIF may have multiple roles in osteogenic induction, as suggested by the paradoxical conclusions. In addition, it is well known that hypoxia increases the expression of angiogenic factors in MSCs, such as VEGF[94]. An initial period of hypoxia is present during the process of bone regeneration in the body, which stimulated the deposition of several factors, such as VEGF and IL-6, and promoted vascularization later on[99]. It has been observed that short-term (7 days) hypoxic conditioning did not retard osteogenic differentiation of stromal vascular fraction-derived cells (SVFC) in bioprinted constructs, but it enhanced the vascularization of SVFC as indicated by increased expression of VEGFA and HIF1A[27]. Given the fact that the hypoxic environment is beneficial for capillary formation, but may also inhibit the differentiation of MSCs into osteoblasts[100-102], an ideal design for bone bioprinting is to provide a hypoxic environment with a controlled oxygen diffusion for the embedded human umbilical vein endothelial cells (HUVECs) so that the oxygen supply to the bone region is not compromised[53].

2.8. Dynamic culture

Mechanical stress continuously remodels bone *in vivo*, and it has been postulated that such stresses are mainly transferred to bone cells through fluid shear stresses[103]. During the loading of a bone, interstitial fluid flows through the pores in the bone, causing a shear stress to be sensed by osteocytes, which are then communicated to osteoblasts and osteoprogenitor cells through their neighboring ECM. During *in vivo* loading, bone cells experience shear forces ranging from 8 to 30 dyn/cm^2[104,105]. Cells can be cultivated in bioreactors with a dynamic environment that mimics the growth conditions of bone, enhancing nutrient transport, exposing cells to fluid shear stresses, and ultimately promoting cell seeding efficiency and differentiation[106,107]. Bioreactors have been shown to benefit bone differentiation and mineralization through mechanical stimulation induced by fluid shear stresses [107-109]. In a study of bone bioprinting, hMSCs were shown to express significantly more COL-I and VEGF when exposed to culture media flowing at a rate of 5 mL/min than when exposed to static culture media[53]. The results of dynamic culture showed superior Ca deposition, an indication that shear stress aided osteogenesis and mineralization. The considerations for bone bioprinting are depicted in Figure 3.

3. Up-to-date progress of bone bioprinting

3.1. Extrusion-based bioprinting of bone

3.1.1. Alginate-based composite bioinks

As a popular biomaterial for bone regeneration, alginate-based composite bioinks have been extensively explored for bone bioprinting. Fedorovich *et al.*[71] conducted an early study in 2008 to examine the bioprinting of Lutrol® F127, agarose, alginate, and methylcellulose hydrogels with an EBB bioprinter and observed that the applied extrusion conditions did not reduce the survival and differentiation capacity of BMSCs. This process was capable of developing bone constructs containing multiple cell types indicated by bioprinting of two fluorescently labeled cell populations within a single scaffold. The authors subsequently created porous constructs which encapsulated two types of cells, namely, EPCs and MSCs[58]. A rectangular 10-layer scaffold, which consisted of two parts (EPC-loaded Matrigel and MSC-loaded Matrigel with the addition of biphasic calcium phosphate [BCP]), demonstrated that cell distribution could be maintained after 2 weeks of culture. Furthermore, the MSC/BCP-laden Matrigel part demonstrated apparent bone formation in immune-deficient mice after 6 weeks of implantation, which demonstrated by Goldner's trichrome and COL-I staining, while cartilage formation was evident in the MSC/Matrigel part as determined by Safranin-O

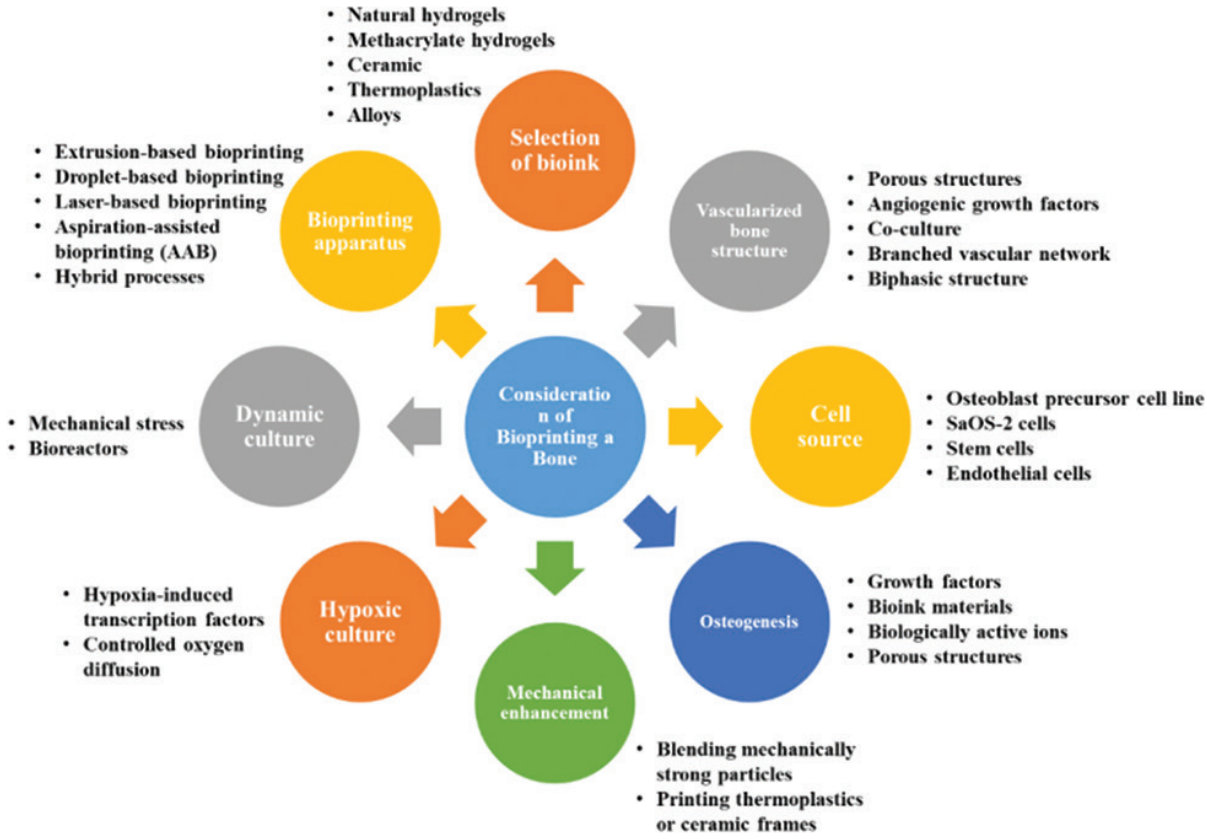

Figure 3. Considerations for bioprinting a bone construct.

and COL-II staining. In another work of the same group, different fiber spacings or angles of fiber deposition were used to fabricate heterogeneous constructs with adjustable porosity (35 – 66%) and elastic modulus (4.7 – 6.6 kPa)[81]. Osteochondral constructs were bioprinted using alginate containing chondrocytes (cartilage compartment) and alginate containing MSCs and osteoinductive BCP particles (bone compartment). As a result, the cell viability of alginate constructs containing human chondrocytes and osteogenic progenitors remained high (90%) during the printing process. Furthermore, chondrogenic and osteogenic differentiation has been demonstrated in different parts of the construct *in vitro* and *in vivo* (subcutaneously in immune-deficient mice).

In a study using a pneumatic EBB system, Loozen *et al.*[110] developed porous or solid constructs containing alginate hydrogel combined with MSCs, BCP particles, and plasmid-DNA-encoding bone morphogenetic protein-2. As a result of plasmid DNA transfection, osteogenic differentiation of cells was observed by enhanced BMP-2 and ALP production, and porous constructs displayed superior BMP-2 production to solid constructs. Bendtsen *et al.*[83] extensively explored the effect of varying materials with different concentrations on their printability, and thus effectively bioprinted mouse calvaria 3T3-E1 (MC3T3) cells within alginate-PVA-HAp bioink, which supported 96% cell viability, indicating that the suspension optimized the printability and improved the cellular activity. Cunniffe *et al.*[111] generated a bioink by combining an arginylglycylaspartic acid (RGD)-γ-irradiated alginate and nano-HAp blended with plasmid DNA (pDNA). The bioprinted constructs containing pDNA showed a higher level of mineralization than those without pDNA. The MSC-encapsulated constructs that were implanted subcutaneously into nude mice demonstrated greater levels of mineral deposition and vascularization compared to cell-free groups.

Cidonio *et al.*[112] developed a bioink composed of synthetic nanoclay (Laponite, LPN) and GelMA, which showed good fidelity and interlinked porosity during EBB. The hBMSCs maintained good viability in the bioprinted construct (86 ± 10% at 21 days of culture), and cell-laden constructs cultured without dexamethasone showed areas of mineralization, indicating the formation of osteogenic tissue. Subsequently, the same team used human BMSCs

encapsulated in a Laponite®-alginate-methylcellulose hydrogel to create bioprint scaffolds, showing 90% cell viability on day 7 of culture with decreased ALP expression and increased calcium mineral deposition over 21 days of culture[113]. MSC-laden scaffolds were implanted in athymic BALB/c mice, where extensive mineralization was observed after 4 weeks of implantation, while bone volume and bone density increased significantly from 2 to 8 weeks. Furthermore, subcutaneous implantation of BMP-2-containing bioprinted scaffolds in mice exhibited increased level of glycosaminoglycans (GAGs) deposition and mineralization.

Alginate is readily processable using cross-linking mechanisms such as ionic interaction, cell cross-linking, photopolymerization, and Schiff-base reaction[114]. The prevalent method for alginate gelation is to combine the alginate with divalent cations, such as Ca^{2+}, Mg^{2+}, Ferrous (Fe^{2+}), Barium (Ba^{2+}), or Sr^{2+}. In the cell cross-linking mechanism, the ligands (e.g., RGD) were grafted onto alginate for cell adhesion[111]. As cells were loaded into the RGD-modified alginate, the receptors on the cell surface can bind to ligands of the modified alginate. In addition, some researchers exploited photopolymerization to solidify methacrylated alginate by employing UV irradiation[115]. Alginate was also prepared in the form of microspheres to deliver growth factors, proteins, and drugs in tissue engineering[114]. Inspired by the advantage of the alginate microsphere, Wu *et al.* embedded the alginate microspheres within the cell aggregates to generate porous tissue strands with high cell density[116]. The incorporation of alginate microspheres facilitated the permeation of oxygen and nutrition, promoting cell viability within the cell aggregates, which offers new insight into scaffold-free biofabrication.

3.1.2. Gelatin-based composite bioinks

As mentioned in **section 2.2.**, bioinks whose main composite is gelatin have also been reported by several studies. Das *et al.*[56] used silk in a bioprinted bone study, where silk fibroin-gelatin (SF-G) bioink was embedded with hTMSC, and *in situ* cytocompatible gelation occurred (enzymatic cross-linking using mushroom tyrosinase and physical cross-linking using sonication). SF-G bioink caused no harm to the cells, and a higher chondrogenic and adipogenic potential was observed in the tyrosinase cross-linked groups, whereas a higher osteogenic differentiation was observed in the sonication cross-linked groups. Using six hydrogel blends of fibrin, gelatin, HA, and glycerol (F/G/H/Gl), Wehrle *et al.*[117] identified the best hydrogel blend which showed high cell viability (>96%) and cell proliferation. The osteogenic differentiation process was carried out in the hydrogels with immortalized hTERT-overexpressing MSCs, fetal MSCs from the umbilical cord MSCs, BMSCs, and ADSCs, among which ADSCs showed the greatest osteogenic differentiation potential indicated by the ALP assay, which were then chosen for bioprinting with the F/G/H/Gl hydrogel. Chiesa *et al.*[118] fabricated a vascularized bone model using gelatin-nanohydroxyapatite (Gel-nHAp), hMSCs, and HUVECs. Gel-nHAp was first extruded followed by hMSCs being seeded on scaffolds and osteogenically differentiated for 2 weeks. Next, lentiviral-GFP transfected HUVECs were placed into the macropores of 3D bioprinted scaffolds. The assembly of a complex capillary-like network was observed, and vascular lumen formation and osteogenic differentiation were confirmed by immunostaining and gene expression.

Although gelatin is easily accessible and has good biocompatibility, its low viscosity, low yield stress, and relatively long cross-linking time during or after bioprinting lead to poor shape retention properties, resulting in difficulty in creating 3D reliable structures with an interconnected pore network[118]. To overcome this obstacle, non-modified gelatin can be bioprinted below the melting temperature (usually below 4°C) to increase the viscosity for extrusion[119] or with the aid of a sacrificial frame to ensure sufficient time for cross-linking with cross-linkers, such as genipin and transglutaminase[118].

3.1.3. Alginate/Gelatin-based composite bioinks

To integrate the benefits of alginate (fast cross-linking) and gelatin (good biocompatibility), alginate/gelatin-based composite bioinks have drawn a lot of attention. As reported by Neufurth *et al.*[75], a polyphosphate Ca salt overlay (polyP·Ca^{2+}-complex) was applied to the bioprinted alginate/gelatine/SaOS-2 cell scaffold to modulate the biological result of the construct. PolyP·Ca^{2+}-complex was surprisingly found to significantly increase the ability of cells to proliferate in the underlining hydrogel. The hardness and mineralization of cell-laden alginate/gelatin hydrogels significantly increased when the overlaid polymer was present. A follow-up study by Wang *et al.*[120] investigated the effect of bioglasses including polyP·Ca^{2+}-complex, silica, and biosilica on the mineralization of SaOS-2 cells embedded in a gelatine/alginate hydrogel. Bioglass particles significantly enhanced the mineralization ability of the entrapped cells, as evidenced by staining with alizarin red S, while element analysis of mineral nodules formed by the SaOS-2 cells indicated a gathering of minerals. Wüst *et al.*[51] took advantage of the thermal gelation of gelatin and the irreversible cross-linking of alginate to develop a two-step process. Cell viability was 85% after 3 days of culture after bioprinting when MSCs were mixed into the hydrogel precursor. Furthermore, a two-phased structure

was produced with a HAp-containing phase and a tubular structure filled with alginate/gelatin to represent bone tissue and vascular structure, respectively.

Different from the blending of alginate and gelatin, alginate/gelatin composite hydrogel has been bioprinted using an *in situ* cross-linking mechanism, which is attributed to the Schiff-base reaction between aldehyde groups of oxidized alginate and amino groups of gelatin[114]. When gelatin was extruded into a support bath that contained oxidized alginate, freeform fabrication of complex 3D structures can be obtained[121].

3.1.4. Photocurable bioinks

Modification of biomaterials (such as gelatin, alginate, and HA) with methacrylate enables chemically cross-linking using UV radiation[122], which overcomes the above-mentioned limitations, such as low viscosity and slow gelation. Photopolymerization has also been integrated into EBB processes to enhance the stability and complexity of the bioprinted bone. In the work by Poldervaart *et al.*[72], MeHA has been investigated for bone bioprinting, where UV light exposure enhanced the storage modulus and elastic modulus of the MeHA, and hBMSCs residing in MeHA hydrogels retained 64% viability after a 21-day culture. Despite the absence of additional osteogenic stimuli, Ca deposition in hydrogels with higher MeHA concentrations (2.5 – 3%) was significantly greater than that observed in hydrogels with lower MeHA concentrations (1.5%). Byambaa *et al.*[52] used GelMA hydrogels containing different concentrations of VEGF to produce a gradient structure, and a gel rod in the center was bioprinted with GelMA, forming a perfusable vascular lumen with an endothelial lining. Cocultured HUVECs and hMSCs reached 93% cell viability after 7 days, and MSCs in the inner fibers differentiated into smooth muscle cells, which promoted vascular vessel formation. In the three outer layers, the MSCs and bioactive silicate nanoplatelets were embedded in GelMA-VEGF bioink, which induced osteogenic differentiation *in vitro*. The Alizarin Red S staining, immunostaining, and RT-qPCR results demonstrated that a mature bone with angiogenesis was generated after 21 days of culture.

3.1.5. Bioinks with particle reinforcement

As biomaterials such as silicate and calcum phosphates are well-known for their roles in increasing mechanical properties and mineralization of bone scaffolds, such materials in the form of particles are supplemented in bioinks. A recent study by Liu *et al.*[123] encapsulated rat BMSCs in a bioink containing nanosilicate (nSi), gelatin, and alginate, in which the addition of nSi resulted in low hydrogel swelling and improved shear-thinning character, storage and loss moduli, and compressive modulus of hydrogels. Hydrogels containing 2% nSi were used for bioprinting and cells could retain their viability and proliferation, accompanied by increased ALP activity and increased gene expression of Runt-related transcription factor 2 (RUNX2), osterix, ALP, collagen type I alpha 1 (COL1A1), OCN, and *osteopontin* (OPN). Critical-sized cranial defects of Sprague Dawley (SD) rats were also transplanted with scaffolds, and micro-CT, Van Gieson, histochemistry, and Masson's trichrome staining results demonstrated that the MSCs-loaded 2% nSi scaffold showed better outcomes than the control groups (without scaffolds or nSi). Using a nanoengineered bioink consisting of GelMA, kappa-carrageenan, and nSi, which formed an ionic-covalent entanglement network, Chimene *et al.*[124] succeeded in bioprinting a hollow cylinder with 150 layers (3 cm in height). The presence of nSi resulted in the increased compression modulus and the significant deposition of GAGs, proteoglycans, Ca, and phosphate in human MSCs post-bioprinting, demonstrating that the bioink could induce endochondral differentiation of MSCs.

In a study by Demirtaş *et al.*[74], chitosan, chitosan-HAp composite, and MC3T3-E1 cells were printed using an EBB, in which alginate and alginate-HAp hydrogels were used as comparisons. With the incorporation of HAp, both chitosan and alginate hydrogels had 3 – 6 folds greater elastic modulus. Spherical morphology of cells was seen in alginate and chitosan hydrogels on day 7 of culture, whereas spread cells were observed in alginate-HAp and chitosan-HAp hydrogels, indicating a positive effect of HAp on cellular morphology. Cells within chitosan-HAp hydrogel expressed higher levels of osteogenic proteins and Ca deposition as compared to other groups. Using BMSCs, RAW264.7 macrophages, gelatin, GelMA, polyethylene glycol (PEG), and BMP-4-loaded mesoporous silica nanoparticles (MSNs) as bioinks, Sun *et al.*[125] demonstrated that MSNs improved the mechanical and shear-thinning properties of the hydrogel. *In vitro* and *in vivo* (implantation in calvarial defects of DM rats) tests were conducted using RAW/BMP-4 scaffolds, where BMP-4-loaded MSNs induced macrophage polarization and inhibited the inflammatory response. Moreover, the BMSC/RAW/BMP-4 group was tested *in vitro*, which indicated that the expression of RUNX2, OPN, and ALP was up-regulated. The *in vivo* results, further, highlighted the superiority of the BMSC/RAW/BMP-4 group over others regarding new bone volume and degree of neovascularization.

In light of the fact that amorphous magnesium phosphates (AMPs) stimulate rapid differentiation and mineralization of pre-osteogenic cells, a shear-thinning and

printable ECM-based bioink containing 2% octapeptide FEFEFKFK with AMP particles (ECM/AMP bioink) were developed[126]. Dental pulp stem cells were added to ECM/AMP bioink and maintained 90% viability after 5 days in bioprinted constructs. In comparison with the AMP-free control group, ECM/AMP constructs showed greater mineralization and increased RUNX2, OPN, and COL1A1 mRNA expression at 21 days without the presence of growth factors. Eight weeks after implanting ECM/AMP constructs in rat cranial defects, a remarkable increase in bone density as well as new bone formation were observed in the defect. Using a microparticulate bioink composed of poly(lactic-co-glycolic acid) (PLGA), PEG, and carboxymethyl cellulose, Sawkins *et al.*[127] achieved a bioprinted construct with mechanical properties comparable to those of human cancellous bone (Young's modulus: 57.3 MPa) and the pore sizes of 65 – 77 μm. Furthermore, the bioprinted constructs released lysozyme for 15 days, and a high level of protein activity was observed for 9 days.

3.1.6. Hybrid constructs with mechanical reinforcement

As mentioned in **section 2.6.**, to obtain a clinically relevant mechanical strength, hybrid constructs are usually fabricated by EBB, such as using a dual-nozzle setup to print mechanical supporting frames along with cell-laden bioinks and coaxial nozzle to print core-shell filaments (Figure 2A). Lee *et al.*[44] demonstrated a hybrid scaffold containing PCL and cell-embedded alginate fibers, where the alginate fibers provided biological functionality to the construct, while the PCL fibers regulated the mechanical properties. Such a design resulted in a notable increase in Young's modulus and ultimate tensile strength compared to alginate-only scaffolds. Furthermore, an integrated tissue-organ printer able to handle several biomaterials (including gelatin, fibrinogen, HA, and PCL) was established by Kang *et al.*[91] to construct human-scale and mechanically-stable tissues. In the process of reconstructing the mandible bone, authors bioprinted an amniotic fluid-derived stem cell-laden hydrogel, a mixture of PCL and TCP, as well as Pluronic F127. Furthermore, rat calvarial bone constructs were generated in a circular shape using human amniotic fluid-derived stem cells (hAFSCs), revealing restored vascularized bone without necrosis at all implant regions, while the control group treated with scaffold only had negligible bone tissue formation. Kuss *et al.*[27] adopted SVFCs, which maintained the characteristics of ECs, in creating bone constructs with PCL/HAp and SVFC-laden MeHA/GelMA bioinks. In a short-term (<21 days) hypoxic culture *in vitro*, osteogenic differentiation of SVFCs was not affected, which, in turn, promoted vascular gene expression of VEGFA and HIF1A. In athymic mice, short-term hypoxia (7-day hypoxia and 14-day normoxia) promoted microvessel formation *in vivo* at 4 weeks and integration with the host vascular network but did not affect osteogenic differentiation of SVFCs, representing the beneficial effects of short-term hypoxia in bone regeneration.

With coaxial EBB, Raja *et al.*[92] created 3D scaffolds that used CDHA (core) and MC3T3-E1 cell-laden alginate (shell), thereby avoiding conventional sintering of ceramics after simultaneous printing of CDHA and the cell-laden hydrogel. Compared to alginate-only scaffolds (0.3 MPa), core/shell scaffolds have a higher compressive modulus (7 MPa), and CDHA-only scaffolds disintegrated after compression, showing that core/shell scaffolds balance the poor mechanical properties of hydrogel with the brittleness of ceramic. Kim *et al.*[84] fabricated an α-TCP/collagen cell-laden scaffold with MC3T3-E1 cells, where a layer of porous α-TCP/collagen fibers without cells was extruded for mechanical stability, followed by deposition of collagen bioinks onto the porous layer, and this process was repeated until a 3D scaffold was obtained. On the bioprinted scaffolds, more viable cells and a more homogenous distribution of cells were found compared with the controls, namely, the cell-laden collagen-only scaffold and α-TCP/collagen scaffold with dipping-loaded cells. Ahlfeld *et al.*[128] prepared biphasic scaffolds by alternately extruding two materials, namely, the cell-laden alginate-methylcellulose blend (ALG/MC) and calcium phosphate cement (CPC). The compression modulus of the biphasic scaffold containing 50% CPC and ALG/MC was much higher than that of the monophasic scaffolds of ALG/MC (31 ± 9 MPa vs. 37 ± 5 kPa). Osteochondral scaffolds were generated with calcified cartilage between CPC and ALG/MC zones, which resembled articular cartilage and subchondral bone, respectively.

Zhai *et al.*[129] developed a biodegradable material (bioink A) composed of poly(ethylene glycol) diacrylate (PEGDA) and laponite nanoclay (PEG-Clay). A structure was created using a two-channel 3D bioprinting method together with another composite (bioink B) composed of rat osteoblasts (ROBs) loaded within HA. Bioink A improved the mechanical properties and cell adhesion, and the release of magnesium and silicon bioactive ions was conducive to the osteogenic differentiation of cells. The bioink B ensured the uniform distribution of cells in the scaffold and a high survival rate (e.g., >95% after 1 day). *In vitro* experiments showed that the ALP activity of ROBs within the PEG4K-Clay scaffolds was remarkable. *In vivo* tibia repair showed that the regenerated bone size using

Table 1. Summary of the studies on extrusion-based bone bioprinting and properties of the constructs

Study	Materials	Cell source	Animal model	Pore size (porosity)	Mechanical reinforcement	Compressive modulus	Viability	Zonal structure
Fedorovich *et al.*[71]	Alginate, Lutrol F127, PEO-PPO-PEO block copolymer, Matrigel, agarose, methylcellulose	BMSCs	---	300 μm	---	---	~70 – 95%	---
Fedorovich *et al.*[58]	Matrigel, alginate, BCP, Lutrol® F127	EPC, MSCs	Female nude mice	---	---	---	---	EPC-laden Matrigel part on the left and MSC-laden Matrigel part with BCP on the right
Fedorovich *et al.*[81]	Alginate, BCP	MSCs, chondrocytes	Female nude mice	0.8, 1.5, 2.0, and 2.5 mm (0, 35%, 48%, and 66%)	---	6.4 – 14.8 kPa	89%	MSC-laden alginate+BCP on the left and chondrocyte-laden alginate on the right
Loozen *et al.*[110]	Alginate, calcium phosphate, plasmid DNA encoding BMP-2	MSCs	Mice	1 mm (40%)	---	Porous: 5.6 kPa Solid: 7.3 kPa	80 – 90%	---
Bendtsen *et al.*[83]	Alginate, PVA, HAp	MC3T3-E2	---	---	---	8.6 – 10.3 kPa	~78 – 96%	---
Cunniffe *et al.*[111]	Alginate (RGD-γ-irradiated), nHAp, PCL, pDNA, BMP-2, TGF-β3	MSCs	Nude mice	---	---	---	~100%	PCL supporting mesh
Cidonio *et al.*[112]	Nanoclay LPN, GelMA	hBMSCs	---	---	---	---	86 ± 10% at 21 days	---
Cidonio *et al.*[113]	LAP, alginate, methylcellulose BMP-2, VEGF	hBMSCs, HUVECs	Male athymic immunodeficient mice	---	---	---	~90%	---
Das *et al.*[56]	Silk fibroin, gelatin	hTMSCs	---	1 mm	---	---	>86%	---
Wehrle *et al.*[117]	Fibrin, gelatin, alginate agarose, collagen, HA, glycerol Hap	iMSCs, ucMSCs, BMSCs, ADSCs	---	---	---	---	~97%	--
Chiesa *et al.*[118]	Type A gelatin, nHAp, genipin	hMSCs, HUVECs	--	--	--	36.4 ± 9.6 kPa	--	--
Neufurth *et al.*[75]	Alginate, gelatin, agarose, polyphosphate+CaCl2 Complex	SaOS-2	---	---		---	92%	---
Wang *et al.*[120]	Alginate, gelatin, polyphosphate+CaCl2 complex, silica, biosilica	SaOS-2	---		---	---	---	---

(Contd...)

Table 1. *(Continued)*

Study	Materials	Cell source	Animal model	Pore size (porosity)	Mechanical reinforcement	Compressive modulus	Viability	Zonal structure
Wüst *et al.*[51]	Alginate, gelatin	MSCs	---	---	HAp	With 8% HAp: 36 kPa; With 4% HAp: 32 kPa; Without HAp: 29 kPa.	85%	---
Poldervaart *et al.*[72]	MeHA	hBMSCs	---	1 mm	---	1.3 – 10.6 kPa	~60 – 75%	---
Byambaa *et al.*[52]	GelMA, VEGF, silicate nanoplatelets	hMSCs and HUVECs	---	---	---	5.7 – 6.5 MPa	~50 – 93%	Bone 3D architecture containing osteogenic and vasculogenic niches
Liu *et al.*[123]	nSi, gelatin and alginate	rBMSCs	SD rats	---	nSi	0%nSi: 46 kPa; 1%nSi: 58 kPa; 2%nSi: 101 kPa; 3%nSi: 214 kPa	---	---
Chimene *et al.*[124]	GelMA, kCA, nSi	hMCS	---	---	nSi	103 kPa	---	---
Demirtaş *et al.*[74]	Chitosan, alginate, HAp	MC3T3-E1	---	100 – 200 μm	HAp particles	Without HAp: 3.5 – 4.6 kPa; With HAp: 15 – 19 kPa	>90%	---
Sun *et al.*[125]	Gelatin, GelMA, PEG, MSNs, BMP-4	BMSCs, RAW264.7 macrophages	Male SD rats	---	MSNs	0% MSNs: 121 kPa 0.4% MSNs: 195 kPa 0.8% MSNs: 233 kPa	>90%	---
Dubey *et al.*[126]	Octapeptide FEFEFKFK, AMP	DPSCs	Male rats	---	---	---	~90%	---
Sawkins *et al.*[127]	PLGA, PEG, CMC, Pluoronic F-127	MSCs	---	65 – 76 μm, (10.8 – 12.4%)	---	54.4 – 57.3 MPa	50 – 87%	---
Lee *et al.*[44]	PCL, alginate	MC3T3-E1	---	300 – 500 μm	PCL struts	8.3 – 15.4 MPa (tensile)	84%	---
Kang *et al.*[91]	Gel composite (gelatin, fibrinogen, HA and glycerol), PCL, TCP, Pluronic F127	hAFSCs, rabbit ear chondrocytes, Mouse C2C12 myoblasts	Rat and athymic mice	70%	PCL, PCL/TCP structures	~30 – 45 MPa	>91%	---
Kuss *et al.*[27]	MeHA, GelMA and HA, PCL/Hap	SVF derived cells	Mice	400 μm	PCL/HAp frame	~55 MPa	---	---
Raja *et al.*[92]	TCP, alginate	MC3T3-E1	---	1.7 mm	TCP strust in the core	Core/shell scaffold: 7 MPa, Alginate scaffold: 0.3 MPa	---	---
Kim *et al.*[84]	TCP, COL-I	MC3T3-E1	---	~500 μm	TCP/collagen struts	Collagen: 0.04 MPa; Construct: 0.55 MPa	>91%	---

(Contd...)

https://doi.org/10.18063/ijb.v9i1.628

Table 1. *(Continued)*

Study	Materials	Cell source	Animal model	Pore size (porosity)	Mechanical reinforcement	Compressive modulus	Viability	Zonal structure
Ahlfeld *et al.*[128]	CPC, ALG/MC	hMCSs	--	--	--	30.7 ± 9.1 MPa	--	--
Zhai *et al.*[129]	PEGDA, Laponite XLG nanoclay, HA	ROBs	Male rats	--	Laponite XLG nanoclay	20% PEG4K-7% Clay: 0.47 MPa 20% PEG10K-7% Clay: 0.98 MPa	>90% at 1 day	--

PEO: Polyethylene glycol, PPO: Poly (phenylene oxide), BCP: Biphasic calcium phosphate, DNA: Deoxyribonucleic acid, BMP-2: Bone morphogenetic protein 2, HAp: Hydroxyapatite, PLGA: Poly (lactic-co-glycolic acid), PEG: Poly (ethylene oxide), CMC: Carboxymethyl cellulose, COL-I: Collagen type I, HA: Hyaluronic acid, PCL: Polycaprolactone, TCP: Tricalcium phosphate, PLA: Polylactic acid, GelMA: Gelatin methacrylate, VEGF: Vascular endothelial growth factor, MeHA: Methacrylated hyaluronic acid, PVA: Polyvinyl alcohol, RGD: Arginylglycylaspartic acid, nHAp: Nano-hydroxyapatite, pDNA: Plasmid DNA, TGF-β3: Transforming growth factor-beta 3, nSi: Nanosilicate, kCA: Kappa-carrageenan, AMP: Amorphous magnesium phosphate, LAP: Laponite, CPC: Calcium phosphate cement, PEGDA: Poly ethylene glycol diacrylate, ALG/MC: Alginate-methylcellulose blend, LPN: Laponite, MSNs : Mesoporous silica nanoparticles, BMP-4: Bone morphogenetic protein 4, MSCs: Mesenchymal stem cells, HUVECs: Human umbilical vein endothelial cells, hTMSCs: Human nasal inferior turbinate tissue-derived MSCs, hAFSCs: Human amniotic fluid-derived stem cells, SVF: Stromal vascular fraction, NHOst: Normal human osteoblasts, iMSCs: Immortalized hTERT-overexpressing MSCs, ucMSCs: Fetal MSCs from umbilical cord, BMSCs: Bone marrow stem cells, ADSCs: Adipose-derived stem cells, rBMSCs: Rat BMSCs, hMSCs: Human MSCs, DPSCs: Dental pulp stem cells, SD: Sprague Dawley, ROBs: Rat osteoblasts

ROB-laden PEG4K-Clay scaffolds was significantly larger than that of other groups.

Table 1 summarizes the studies on extrusion-based bone bioprinting and the properties of the bioprinted bone constructs.

3.2. Droplet-based bioprinting of bone

Campos *et al.*[130] applied DBB to bone reconstruction, and thermo-responsive agarose hydrogels with COL-I were inkjet-printed at different concentrations. By increasing the agarose content in agarose/collagen composites, more precise contours could be captured in the bioprinted tissue, since the viscosity and mechanical stiffness of the bioinks were improved, therefore facilitating their printability. However, softer hydrogels resulted in the greater elongation of MSCs after osteogenic differentiation. Cells survived in the bioprinting and preserved the mesenchymal phenotype, as confirmed by high cell viability (>98%), immunostaining of vimentin+ and CD34−, ALP activity, and bone-related gene expression.

3.3. Laser-based bioprinting of bone

Using the digital light processing-based 3D bioprinting technique, Anada *et al.*[131] generated a construct that consists of two rings, which are an outer ring of octacalcium phosphate (OCP) and GelMA imitating the cortical shell as well as an inner ring of HUVEC spheroids and GelMA imitating the bone marrow. On increasing the concentration of OCP, MSC differentiation was enhanced, resulting in increased ALP activity, and the vascularization was observed in hydrogels, which contained HUVEC spheroids in combination with GelMA.

Bernal *et al.*[132] developed an optical-tomography-inspired volumetric printing (VBP) apparatus, which enables structures of complex shapes to be bioprinted within seconds, and used in bone remodeling. This method overcomes the limitations of bioprinting such as a long printing time and difficulty of printing complex structures. It was used to bioprint an anatomical bone trabecular model containing MSCs, in which the smallest feature was 145 μm, and endothelial colony-forming cells (ECFCs) and MSCs were further added into the pores to form a heterocellular structure, where the vascular formation was seen after a 3-day culture.

3.4. Aspiration-assisted bioprinting of bone

Heo *et al.*[133] used AAB technology to control the precise printing of osteogenically differentiated hMSC/HUVEC spheroids. The method allowed the printed spheroids to tightly self-assemble and retain their original shape without disintegration. The survival rate of cells in hMSC/HUVEC

Table 2. Summary of the studies on bone bioprinting using DBB, LBB, and AAB

Study	Technology	Materials	Cell source	Animal model	Pore size (porosity)	Mechanical reinforcement	Compressive modulus	Viability	Zonal structure
Duarte Campos *et al.*[130]	Inkjet	COL-I, agarose	MSCs	---	---	---	18.1, 53.1 and 89.1 kPa	98% at 21 days	---
Anada *et al.*[131]	SLA	OCP, GelMA	HUVECs	---	---	---	---	---	Peripheral OCP-containing GelMA ring + central GelMA ring containing HUVEC spheroids
Bernal *et al.*[132]	VBP	GelMA	ACPCs, MSCs, ECFCs	---	---	---	266 kPa	>85%	---
Heo *et al* [133]	AAB	Cell spheroid	hMSCs, HUVECs	---	---	---	---	>85%	---

SLA: Stereolithography, VBP: Volumetric bioprinting, AAB: Aspiration-assisted bioprinting, COL-I: Collagen type I, GelMA: Gelatin methacrylate, OCP: Octacalcium phosphate, MSCs: Mesenchymal stem cells, HUVECs: Human umbilical vein endothelial cells, ACPCs: Articular Cartilage-resident chondroprogenitor cells, ECFCs: Endothelial colony forming cells, hMSCs: Human MSCs

Table 3. Summary of the studies on bone bioprinting using hybrid processes

Study	Technology	Materials	Cell source	Animal model	Pore size (porosity)	Mechanical reinforcement	Compressive modulus	Zonal structure
Cui *et al.*[53]	Extrusion+ SLA	PLA, GelMA, BMP-2 and VEGF peptides	hMSCs and HUVECs	---	260 μm (20%)	PLA fibers	Construct: 0.38 GPa; Hydrogel: 10 – 30 kPa	Vascularized construct with capillary networks
Rukavina *et al.*[134]	Extrusion + DoD	Fibrinogen, Gelatin, HA, Glycerol, VEGF, bFGF, HAp, PCL	HUVECs ADSCs	SCID mice	---	---	---	PCL frame

SLA: Stereolithography, DoD: Drop-on-demand, PLA: Polylactic acid, GelMA: Gelatin methacrylate, BMP-2: Bone morphogenetic protein 2, VEGF: Vascular endothelial growth factor, HA: Hyaluronic acid, bFGF: basic fibroblast growth factor, HAp: Hydroxyapatite, PCL: Polycaprolactone, hMSCs: Human mesenchymal stem cells, HUVECs: Human umbilical vein endothelial cells, ADSCs: Adipose-derived stem cells

spheroids was significantly higher than that in hMSC-only spheroids. The addition of HUVECs also promoted the osteogenic differentiation of cells. The hMSC/HUVEC spheroids showed a higher expression of COL1, ALP, and bone sialoprotein (BSP) compared to control groups (2D cultured hMSC and hMSC-only spheroids). This strategy provided a new possibility for printing bone tissue with anatomically-relevant cell density. Table 2 summarizes the above-mentioned studies on bone bioprinting using DBB, LBB, and AAB and the properties of the bioprinted bone constructs.

3.5. Hybrid bioprinting of bone

To replicate a bone construct with interior vascular networks, hybrid bioprinting processes which integrated EBB and LBB or DBB have been reported. Cui *et al.*[53] used a hybrid bioprinting platform composed of FDM and SLA. Using this technique, they deposited polylactide (PLA) fibers and GelMA hydrogel to reproduce a vascularized Haversian system of bone tissue. In the manufacturing process, the polydopamine (pDA)-coated PLA scaffold (bone region) was immobilized with BMP-2 peptides, and then, VEGF peptides were conjugated to GelMA chains (vascular region). PLA scaffolds were pre-seeded with hMSCs, whereas hMSCs and HUVECs were embedded at a 1:1 ratio in the GelMA hydrogel, where the pDA- and BMP-2-modification was found to promote cell growth and spread on the scaffold and the BMP-2 benefited osteogenesis. In a dynamic culture of perfusion, notable osteogenesis and the formation of vascular networks can be observed, as indicated by the higher expression of COL-I, Ca deposition, and VEGF than in static culture.

Combined bioprinting of ADSCs and HUVECs has also been reported to promote vascularization in bioprinted bone tissue[134]. ADSCs underwent osteogenic differentiation

for 7 days before being added into the hydrogel composite (containing fibrinogen, gelatin, HA, glycerol, HAp, VEGF, basic fibroblast growth factor [bFGF], and aprotinin), which was subsequently extruded. An array of droplets was deposited through drop-on-demand bioprinting of HUVECs-loaded hydrogel composite (including fibrinogen, VEGF, bFGF, and aprotinin) after every second layer of ADSC-laden bioink was printed. The bioprinted construct was enclosed by a PCL frame to ease transportation and was, then, implanted subcutaneously into mice. On 12-day implantation, large volumes of calcified ECM, as well as blood vessels with lumens, were observed. Table 3 summarizes the above-mentioned studies on bone bioprinting using hybrid processes and the properties of the bioprinted bone constructs.

4. Conclusion and future prospects

The advancement of bone bioprinting with the use of various hydrogels, cell types, and other osteoconductive components has recently been remarkable, with several studies presenting mineralized structures with the vascularized network. It takes a considerable period (until the healing and remodeling process is complete) to create a durable structure with appropriate mechanical properties and physiological functions, which requires a balance between bioink degradation and tissue regeneration[135]. It is also challenging to develop large-scale vascularized bone grafts that meet the requirements of the clinical setting and easy integration with host tissue[136]. As discussed herein, researchers are striving to provide solutions to tackle the limitations in bone bioprinting, and it is recommended that constant efforts are made to integrate acellular scaffolds with cellular bioinks to modify the mechanical properties of bioprinted bone[13]. It is anticipated that more advanced processes and bioprinters will be developed that can deposit both cellular and non-cellular biomaterials with high efficiency, biocompatibility, and control over printing conditions (e.g., temperature, oxygen tension, and humidity). The piezoelectric nature of bone aids in promoting bone adaptation and remodeling by electromechanical mechanisms[137]. Hence, the addition of electromagnetic materials as a means of controlling the microenvironment of bioprinted bone might prove to be an effective avenue in the future when it comes to discovering new bioinks for bone bioprinting. For instance, currently available bioinks can be incorporated with conduction polymers, such as carbon nanotubes and graphene, to provide structural stability, guide cell growth, as well as stimulate bone formation[138]. A large number of biomaterials are expected to be developed in the future to achieve functional 3D bone bioprinting, which can be achieved with the integration of multidisciplinary knowledge and continuous financial support.

Acknowledgment

None.

Funding

This work was funded by the National Natural Science Foundation of China (grant number 52205305), the GuangDong Basic and Applied Basic Research Foundation (grant number 2020A1515110724), and the Open Foundation of the State Key Laboratory of Fluid Power and Mechatronic Systems (grant number: GZKF-202004).

Conflict of interest

The authors declare no potential conflicts of interest concerning the research, authorship, and/or publication of this article.

Author contributions

Conceptualization: Yang Wu
Funding acquisition: Yang Wu
Visualization: Yang Wu, Ming Li
Writing - original draft: Yang Wu, Ming Li, Hao Su
Writing - review & editing: Yang Wu, Ming Li, Hao Su, Huaying Chen, Yonggang Zhu

References

1. Eliaz N, Metoki N, 2017, Calcium phosphate bioceramics: a review of their history, structure, properties, coating technologies and biomedical applications. *Materials* (*Basel*), 10: 334.

   https://doi.org/10.3390/ma10040334

2. Fratzl P, Weinkamer R, 2007, Nature's hierarchical materials. *Prog Mater Sci*, 52: 1263–1334.

   https://doi.org/10.1016/j.pmatsci.2007.06.001

3. Koester KJ, Ager J, Ritchie R, 2008, The true toughness of human cortical bone measured with realistically short Cracks. *Nat Mater*, 7: 672–677.

   https://doi.org/10.1038/nmat2221

4. Rho JY, Kuhn-Spearing L, Zioupos P, 1998, Mechanical properties and the hierarchical structure of bone. *Med Eng Phys*, 20: 92–102.

   https://doi.org/10.1016/s1350-4533(98)00007-1

5. Ke P, Jiao XN, Ge XH, *et al.*, 2014, From macro to micro: Structural biomimetic materials by electrospinning. *RSC Adv*, 4: 39704–39724.

   https://doi.org/10.1039/C4RA05098C

6. Vallet-Regí M, Navarrete DA, Arcos D, 2008, Biomimetic nanoceramics in clinical use: from materials to applications. London, UK: Royal society of chemistry.

7. Florencio-Silva R, Sasso GR, Sasso-Cerri E, *et al.*, 2015, Biology of bone tissue: Structure, function, and factors that influence bone cells. *Biomed Res Int*, 2015: 421746.

   https://doi.org/10.1155/2015/421746

8. Murugan R, Ramakrishna S, 2005, Development of nanocomposites for bone grafting. *Compos Sci Technol*, 65: 2385–2406.

9. Bonfield W, Wang M, Tanner K, 1998, Interfaces in analogue biomaterials. *Acta Mater*, 46: 2509–2518.

10. Atala A, 2000, Tissue engineering for bladder substitution. *World Journal of Urology*, 18: 364–370.

    https://doi.org/10.1007/s003450000152

11. Melchels F, Domingos M, Klein TJ, *et al.*, 2012, Additive manufacturing of tissues and organ. *Prog Polym Sci*, 37: 1079–1104.

12. Bigham A, Foroughi F, Ghomi ER, *et al.*, 2020, The journey of multifunctional bone scaffolds fabricated from traditional toward modern techniques. *Bio Des Manuf*, 3: 281–306.

13. Ashammakhi N, Hasan A, Kaarela O, *et al.*, 2019, Advancing frontiers in bone bioprinting. *Adv Healthc Mater*, 8: 1801048.

14. Lee JM, Yeong WY, 2016, Design and printing strategies in 3D bioprinting of cell-hydrogels: A review. *Adv Healthc Mater*, 5: 2856–2865.

    https://doi.org/10.1002/adhm.201600435

15. Gudapati H, Dey M, Ozbolat I, 2016, A comprehensive review on droplet-based bioprinting: Past, present and future. *Biomaterials*, 102: 20–42.

    https://doi.org/10.1016/j.biomaterials.2016.06.012

16. Koch L, Gruene M, Unger C, *et al.*, 2013, Laser assisted cell printing. *Curr Pharm Biotechnol*, 14: 91–97.

17. Guillotin B, Ali M, Ducom A, *et al.*, 2013, Laser-assisted bioprinting for tissue engineering. In: Forgacs g, sun w, editors. Biofabrication micro and nano-fabrication printing patterning assem. Boston: william andrew publishing. p95–p118.

18. Ayan B, Heo DN, Zhang Z, *et al.*, 2020, Aspiration-assisted bioprinting for precise positioning of biologics. *Sci Adv*, 6: eaaw5111.

    https://doi.org/10.1126/sciadv.aaw5111

19. Lee KY, Mooney DJ, 2012, Alginate: properties and biomedical applications. *Prog Polym Sci*, 37: 106–126.

    https://doi.org/10.1016/j.progpolymsci.2011.06.003

20. Funakoshi T, Majima T, Iwasaki N, *et al.*, 2005, Application of tissue engineering techniques for rotator cuff regeneration using a chitosan-based hyaluronan hybrid fiber scaffold. *Am J Sports Med*, 33: 1193–1201.

    https://doi.org/10.1177/0363546504272689

21. Laranjeira M, Domingues RM, Costa-Almeida R, *et al.*, 2017, 3D mimicry of native-tissue-fiber architecture guides tendon-derived cells and adipose stem cells into artificial tendon constructs. *Small*, 13: 1700689.

    https://doi.org/10.1002/smll.201700689

22. Nichol JW, Koshy ST, Bae H, *et al.*, 2010, Cell-laden microengineered gelatin methacrylate hydrogels. *Biomaterials*, 31: 5536–5544.

    https://doi.org/10.1016/j.biomaterials.2010.03.064

23. Yue K, Trujillo-de Santiago G, Alvarez MM, *et al.*, 2015, Synthesis, properties, and biomedical applications of gelatin methacryloyl (GelMA) hydrogels. *Biomaterials*, 73: 254–271.

    https://doi.org/10.1016/j.biomaterials.2015.08.045

24. Klotz BJ, Gawlitta D, Rosenberg AJ, *et al.*, 2016, Gelatin-methacryloyl hydrogels: Towards biofabrication-based tissue repair. *Trends Biotechnol*, 34: 394–407.

    https://doi.org/10.1016/j.tibtech.2016.01.002

25. D O'Connell C, Di Bella C, Thompson F, *et al.*, 2016, Development of the biopen: A handheld device for surgical printing of adipose stem cells at a chondral wound site. *Biofabrication*, 8: 015019.

    https://doi.org/10.1088/1758-5090/8/1/015019

26. Evinger AJ, Jeyakumar JM, Hook LA, *et al.*, 2013, Osteogenic differentiation of mesenchymal stem/stromal cells within 3D bioprinted neotissues. *FASEB J*, 27: 193.

27. Kuss MA, Harms R, Wu S, *et al.*, 2017, Short-term hypoxic preconditioning promotes prevascularization in 3D bioprinted bone constructs with stromal vascular fraction derived cells. *RSC Adv*, 7: 29312–29320.

    https://doi.org/10.1039/C7RA04372D

28. Schuurman W, Khristov V, Pot MW, *et al.*, 2011, Bioprinting of hybrid tissue constructs with tailorable mechanical Properties. *Biofabrication*, 3: 021001.

    https://doi.org/10.1088/1758-5082/3/2/021001

29. Cohen DL, Malone E, Lipson H, *et al.*, 2006, Direct freeform fabrication of seeded hydrogels in arbitrary geometries. *Tissue Eng*, 12: 1325–1335.

    https://doi.org/10.1089/ten.2006.12.1325

30. Schagemann J, Chung H, Mrosek E, *et al.*, 2010, Poly-∈-caprolactone/gel hybrid scaffolds for cartilage tissue engineering. *J Biomed Mater Res A*, 93: 454–463.

    https://doi.org/10.1002/jbm.a.32521

31. Endres M, Hutmacher D, Salgado A, *et al.*, 2003, Osteogenic induction of human bone marrow-derived mesenchymal progenitor cells in novel synthetic polymer-hydrogel matrices. *Tissue Eng*, 9: 689–702.

    https://doi.org/10.1089/107632703768247386

32. Park JW, Shin YC, Kang HG, *et al.*, 2021, *In Vivo* analysis of post-joint-preserving surgery fracture of 3D-printed

ti-6al-4v implant to treat bone Cancer. *Bio Des Manuf*, 4: 879–888.

33. Li X, Yuan Y, Liu L, *et al.*, 2020, 3D printing of hydroxyapatite/tricalcium phosphate scaffold with hierarchical porous structure for bone regeneration. *Bio Des Manuf*, 3: 15–29.

34. Dong Y, Duan H, Zhao N, *et al.*, 2018, Three-dimensional printing of β-tricalcium phosphate/calcium silicate composite scaffolds for bone tissue engineering. *Bio Des Manuf*, 1: 146–156.

35. Zhang B, Sun H, Wu L, *et al.*, 2019, 3D printing of calcium phosphate bioceramic with tailored biodegradation rate for skull bone tissue reconstruction. *Bio Des Manuf*, 2: 161–171.

36. Oladapo BI, Zahedi SA, Ismail SO, *et al.*, 2021, 3D printing of peek-chap scaffold for medical bone implant. *Bio Des Manuf*, 4: 44–59.

37. Wang X, Schröder HC, Wang K, *et al.*, 2012, Genetic, biological and structural hierarchies during sponge spicule formation: From soft sol-gels to solid 3d silica composite structures. *Soft Matter*, 8: 9501–9518.

38. Wiens M, Wang X, Schröder HC, *et al.*, 2010, The role of biosilica in the osteoprotegerin/rankl ratio in human osteoblast-like cells. *Biomaterials*, 31: 7716–7725.

https://doi.org/10.1016/j.biomaterials.2010.07.002

39. Nguyen LH, Annabi N, Nikkhah M, *et al.*, 2012, Vascularized bone tissue engineering: Approaches for potential improvement. *Tissue Eng Part B Rev*, 18: 363–382.

https://doi.org/10.1089/ten.TEB.2012.0012

40. Oryan A, Alidadi S, Moshiri A, *et al.*, 2014, Bone regenerative medicine: Classic options, novel strategies, and future directions. *J Orthop Surg Res*, 9: 18.

https://doi.org/10.1186/1749-799X-9-18

41. Wang J, Yang M, Zhu Y, *et al.*, 2014, Phage nanofibers induce vascularized osteogenesis in 3D printed bone scaffolds. *Adv Mater*, 26: 4961–4966.

https://doi.org/10.1002/adma.201400154

42. Wang MO, Vorwald CE, Dreher ML, *et al.*, 2015, Evaluating 3D-printed biomaterials as scaffolds for vascularized bone tissue engineering. *Adv Mater*, 27: 138–144.

https://doi.org/10.1002/adma.201403943

43. Whang K, Healy K, Elenz D, *et al.*, 1999, Engineering bone regeneration with bioabsorbable scaffolds with novel microarchitecture. *Tissue Eng*, 5: 35–51.

https://doi.org/10.1089/ten.1999.5.35

44. Lee H, Ahn S, Bonassar LJ, *et al.*, 2013, Cell (MC3T3-E1)-printed poly (∈-caprolactone)/alginate hybrid scaffolds for tissue regeneration. *Macromol Rapid Commun*, 34: 142–149.

https://doi.org/10.1002/marc.201200524

45. Amini AR, Laurencin CT, Nukavarapu SP, 2012, Differential analysis of peripheral blood-and bone marrow-derived endothelial progenitor cells for enhanced vascularization in bone tissue engineering. *J Orthop Res*, 30: 1507–1515.

https://doi.org/10.1002/jor.22097

46. Samorezov JE, Alsberg E, 2015, Spatial regulation of controlled bioactive factor delivery for bone tissue engineering. *Adv Drug Deliv Rev*, 84: 45–67.

https://doi.org/10.1016/j.addr.2014.11.018

47. Santos MI, Reis RL, 2010, Vascularization in bone tissue engineering: Physiology, current strategies, major hurdles and future challenges. *Macromol Biosci*, 10: 12–27.

https://doi.org/10.1002/mabi.200900107

48. Kirkpatrick CJ, Fuchs S, Unger RE, 2011, Co-culture systems for vascularization-learning from nature. *Adv Drug Deliv Rev*, 63: 291–299.

https://doi.org/10.1016/j.addr.2011.01.009

49. Brennan MA, Davaine JM, Layrolle P, 2013, Pre-vascularization of bone tissue-engineered constructs. *Stem Cell Res Ther*, 4: 1–3.

https://doi.org/10.1186/scrt307

50. Mishra R, Roux BM, Posukonis M, *et al.*, 2016, Effect of prevascularization on *in vivo* vascularization of poly (propylene fumarate)/fibrin scaffolds. *Biomaterials*, 77: 255–266.

https://doi.org/10.1016/j.biomaterials.2015.10.026

51. Wüst S, Godla ME, Müller R, *et al.*, 2014, Tunable hydrogel composite with two-step processing in combination with innovative hardware upgrade for cell-based three-dimensional bioprinting. *Acta Biomater*, 10: 630–640.

https://doi.org/10.1016/j.actbio.2013.10.016

52. Byambaa B, Annabi N, Yue K, *et al.*, 2017, Bioprinted osteogenic and vasculogenic patterns for engineering 3D bone tissue. *Adv Healthc Mater*, 6: 1700015.

https://doi.org/10.1002/adhm.201700015

53. Cui H, Zhu W, Nowicki M, *et al.*, 2016, Hierarchical fabrication of engineered vascularized bone biphasic constructs via dual 3D bioprinting: Integrating regional bioactive factors into architectural design. *Adv Healthc Mater*, 5: 2174–2181.

https://doi.org/10.1002/adhm.201600505

54. Rodan SB, Imai Y, Thiede MA, *et al.*, 1987, Characterization of a human osteosarcoma cell line (saos-2) with osteoblastic properties. *Cancer Res*, 47: 4961–4966.

55. Hausser HJ, Brenner RE, 2005, Phenotypic instability of saos-2 cells in long-term culture. *Biochem Biophys Res Commun*, 333: 216–222.

https://doi.org/10.1016/j.bbrc.2005.05.097

56. Das S, Pati F, Choi YJ, *et al.*, 2015, Bioprintable, cell-laden

silk fibroin-gelatin hydrogel supporting multilineage differentiation of stem cells for fabrication of three-dimensional tissue constructs. *Acta Biomater*, 11: 233–246.

https://doi.org/10.1016/j.actbio.2014.09.023

57. Sabapathy V, Kumar S, 2016, hiPSC-derived iMSCs: NextGen MSCs as an advanced therapeutically active cell resource for regenerative medicine. *J Cell Mol Med*, 20: 1571–1588.

https://doi.org/10.1111/jcmm.12839

58. Fedorovich NE, Wijnberg HM, Dhert WJ, *et al.*, 2011, Distinct tissue formation by heterogeneous printing of osteo-and endothelial progenitor cells. *Tissue Eng Part A*, 17: 2113–2121.

https://doi.org/10.1089/ten.TEA.2011.0019

59. Gruene M, Pflaum M, Hess C, *et al.*, 2011, Laser printing of three-dimensional multicellular arrays for studies of cell-cell and cell-environment interactions. *Tissue Eng Part C Methods*, 17: 973–982.

https://doi.org/10.1089/ten.TEC.2011.0185

60. Merfeld-Clauss S, Gollahalli N, March KL, *et al.*, 2010, Adipose tissue progenitor cells directly interact with endothelial cells to induce vascular network formation. *Tissue Eng Part A*, 16: 2953–2966.

https://doi.org/10.1089/ten.tea.2009.0635

61. Wu Y, Chen L, Scott PG, *et al.*, 2007, Mesenchymal stem cells enhance wound healing through differentiation and angiogenesis. *Stem cells*, 25: 2648–2659.

https://doi.org/10.1634/stemcells.2007-0226

62. Pederson L, Ruan M, Westendorf JJ, *et al.*, 2008, Regulation of bone formation by osteoclasts involves wnt/bmp signaling and the chemokine sphingosine-1-phosphate. *Proc Natl Acad Sci U S A*, 105: 20764–20769.

https://doi.org/10.1073/pnas.0805133106

63. Guihard P, Danger Y, Brounais B, *et al.*, 2012, Induction of osteogenesis in mesenchymal stem cells by activated monocytes/macrophages depends on oncostatin m signaling. *Stem cells*, 30: 762–772.

https://doi.org/10.1002/stem.1040

64. Albrektsson T, Johansson C, 2001, Osteoinduction, osteoconduction and osseointegration. *Eur Spine J*, 10: S96–S101.

https://doi.org/10.1007/s005860100282

65. Brydone A, Meek D, Maclaine S, 2010, Bone grafting, orthopaedic biomaterials, and the clinical need for bone engineering. *Proc Inst Mech Eng H*, 224: 1329–1343.

https://doi.org/10.1243/09544119JEIM770

66. Dimitriou R, Jones E, McGonagle D, *et al.*, 2011, Bone regeneration: Current concepts and future directions. *BMC Med*, 9: 1–10.

67. Fratzl P, Gupta H, Paschalis E, *et al.*, 2004, Structure and mechanical quality of the collagen-mineral nano-composite in bone. *J Mater Chem*, 14: 2115–2123.

https://doi.org/10.1039/B402005G

68. Kreimendahl F, Köpf M, Thiebes AL, *et al.*, 2017, Three-dimensional printing and angiogenesis: tailored agarose-type i collagen blends comprise three-dimensional printability and angiogenesis potential for tissue-engineered substitutes. *Tissue Eng Part C Methods*, 23: 604–615.

https://doi.org/10.1089/ten.TEC.2017.0234

69. Karageorgiou V, Meinel L, Hofmann S, *et al.*, 2004, Bone morphogenetic protein-2 decorated silk fibroin films induce osteogenic differentiation of human bone marrow stromal cells. *J Biomed Mater Res A*, 71: 528–537.

https://doi.org/10.1002/jbm.a.30186

70. Zhao L, Jiang S, Hantash BM, 2010, Transforming growth factor β1 induces osteogenic differentiation of murine bone marrow stromal cells. *Tissue Eng Part A*, 16: 725–733.

https://doi.org/10.1089/ten.TEA.2009.0495

71. Fedorovich NE, De Wijn JR, Verbout AJ, *et al.*, 2008, Three-dimensional fiber deposition of cell-laden, viable, patterned constructs for bone tissue printing. *Tissue Eng Part A*, 14: 127–133.

https://doi.org/10.1089/ten.a.2007.0158

72. Poldervaart MT, Goversen B, De Ruijter M, *et al.*, 2017, 3D bioprinting of methacrylated hyaluronic acid (MeHA) hydrogel with intrinsic osteogenicity. *PLoS One*, 12: e0177628.

https://doi.org/10.1371/journal.pone.0177628

73. McBeth C, Lauer J, Ottersbach M, *et al.*, 2017, 3D bioprinting of gelma scaffolds triggers mineral deposition by primary human osteoblasts. *Biofabrication*, 9: 015009.

https://doi.org/10.1088/1758-5090/aa53bd

74. Demirtaş TT, Irmak G, Gümüşderelioğlu M, 2017, A bioprintable form of chitosan hydrogel for bone tissue engineering. *Biofabrication*, 9: 035003.

https://doi.org/10.1088/1758-5090/aa7b1d

75. Neufurth M, Wang X, Schröder HC, *et al.*, 2014, Engineering a morphogenetically active hydrogel for bioprinting of bioartificial tissue derived from human osteoblast-like saos-2 cells. *Biomaterials*, 35: 8810–8819.

https://doi.org/10.1016/j.biomaterials.2014.07.002

76. Pan Q, Gao C, Wang Y, *et al.*, 2020, Investigation of bone reconstruction using an attenuated immunogenicity xenogenic composite scaffold fabricated by 3D printing. *Bio Des Manuf*, 3: 396–409.

77. Golafshan N, Vorndran E, Zaharievski S, *et al.*, 2020, Tough

magnesium phosphate-based 3D-printed implants induce bone regeneration in an equine defect model. *Biomaterials*, 261: 120302.

https://doi.org/10.1016/j.biomaterials.2020.120302

78. Liu D, Nie W, Li D, *et al.*, 2019, 3D Printed PCL/SrHA scaffold for enhanced bone regeneration. *Chem Eng J*, 362: 269–279.

79. Sun H, Hu C, Zhou C, *et al.*, 2020, 3D Printing of calcium phosphate scaffolds with controlled release of antibacterial functions for jaw bone repair. *Mater Des*, 189: 108540.

https://doi.org/10.1016/j.matdes.2020.108540

80. e Silva EP, Huang B, Helaehil JV, *et al.*, 2021, *In Vivo* study of conductive 3D printed pcl/mwcnts scaffolds with electrical stimulation for bone tissue engineering. *Bio Des Manuf*, 4: 190–202.

81. Fedorovich NE, Schuurman W, Wijnberg HM, *et al.*, 2012, Biofabrication of osteochondral tissue equivalents by printing topologically defined, cell-laden hydrogel scaffolds. *Tissue Eng Part C Methods*, 18: 33–44.

https://doi.org/10.1089/ten.TEC.2011.0060

82. Shoichet MS, Li RH, White ML, *et al.*, 1996, Stability of hydrogels used in cell encapsulation: an *in vitro* comparison of alginate and agarose. *Biotechnol Bioeng*, 50: 374–381.

https://doi.org/10.1002/(SICI)1097-0290(19960520)50:4<374::AID-BIT4>3.0.CO;2-I

83. Bendtsen ST, Quinnell SP, Wei M, 2017, Development of a novel alginate-polyvinyl alcohol-hydroxyapatite hydrogel for 3D bioprinting bone tissue engineered scaffolds. *J Biomed Mater Res A*, 105: 1457–1468.

https://doi.org/10.1002/jbm.a.36036

84. Kim WJ, Yun HS, Kim GH, 2017, An innovative cell-laden α-tcp/collagen scaffold fabricated using a two-step printing process for potential application in regenerating hard tissues. *Sci Rep*, 7: 3181.

https://doi.org/10.1038/s41598-017-03455-9

85. Mishra R, Basu B, Kumar A, 2009, Physical and cytocompatibility properties of bioactive glass-polyvinyl alcohol-sodium alginate biocomposite foams prepared via sol-gel processing for trabecular bone regeneration. *J Mater Sci Mater Med*, 20: 2493–500.

https://doi.org/10.1007/s10856-009-3814-1

86. Costa JB, Silva-Correia J, Pina S, *et al.*, 2019, Indirect printing of hierarchical patient-specific scaffolds for meniscus tissue engineering. *Bio Des Manuf*, 2: 225–241.

87. Wang Q, Ma Z, Wang Y, *et al.*, 2021, Fabrication and characterization of 3D printed biocomposite scaffolds based on pcl and zirconia nanoparticles. *Bio Des Manuf*, 4: 60–71.

88. Askari E, Rasouli M, Darghiasi SF, *et al.*, 2021, Reduced graphene oxide-grafted bovine serum albumin/bredigite nanocomposites with high mechanical properties and excellent osteogenic bioactivity for bone tissue engineering. *Bio Des Manuf*, 4: 243–257.

89. Lee CH, Rodeo SA, Fortier LA, *et al.*, 2014, Protein-releasing polymeric scaffolds induce fibrochondrocytic differentiation of endogenous cells for knee meniscus regeneration in sheep. *Sci Transl Med*, 6: 266ra171.

https://doi.org/10.1126/scitranslmed.3009696

90. Ding C, Qiao Z, Jiang W, *et al.*, 2013, Regeneration of a goat femoral head using a tissue-specific, biphasic scaffold fabricated with cad/cam technology. *Biomaterials*, 34: 6706–6716.

https://doi.org/10.1016/j.biomaterials.2013.05.038

91. Kang HW, Lee SJ, Ko IK, *et al.*, 2016, A 3D bioprinting system to produce human-scale tissue constructs with structural integrity. *Nat Biotechnol*, 34: 312–319.

https://doi.org/10.1038/nbt.3413

92. Raja N, Yun HS, 2016, A simultaneous 3D printing process for the fabrication of bioceramic and cell-laden hydrogel core/shell scaffolds with potential application in bone tissue regeneration. *J Mater Chem B*, 4: 4707–4716.

https://doi.org/10.1039/C6TB00849F

93. Araldi E, Schipani E, 2010, Hypoxia, HIFs and bone development. *Bone*, 47: 190–196.

https://doi.org/10.1016/j.bone.2010.04.606

94. Fan W, Crawford R, Xiao Y, 2010, Enhancing *In Vivo* vascularized bone formation by cobalt chloride-treated bone marrow stromal cells in a tissue engineered periosteum model. *Biomaterials*, 31: 3580–3589.

https://doi.org/10.1016/j.biomaterials.2010.01.083

95. Mamalis AA, Cochran DL, 2011, The therapeutic potential of oxygen tension manipulation via hypoxia inducible factors and mimicking agents in guided bone regeneration. A Review. *Arch Oral Biol*, 56: 1466–1475.

https://doi.org/10.1016/j.archoralbio.2011.05.001

96. Boyette LB, Creasey OA, Guzik L, *et al.*, 2014, Human bone marrow-derived mesenchymal stem cells display enhanced clonogenicity but impaired differentiation with hypoxic preconditioning. *Stem Cells Transl Med*, 3: 241–254.

https://doi.org/10.5966/sctm.2013-0079

97. Merceron C, Vinatier C, Portron S, *et al.*, 2010, Differential effects of hypoxia on osteochondrogenic potential of human adipose-derived stem cells. *Am J Physiol Cell Physiol*, 298: C355–C364.

https://doi.org/10.1152/ajpcell.00398.2009

98. Utting J, Robins S, Brandao-Burch A, *et al.*, 2006, Hypoxia inhibits the growth, differentiation and bone-forming capacity of rat osteoblasts. *Exp Cell Res*, 312: 1693–1702.

https://doi.org/10.1016/j.yexcr.2006.02.007

99. Haque N, Rahman MT, Abu Kasim NH, *et al.*, 2013, Hypoxic culture conditions as a solution for mesenchymal stem cell based regenerative Therapy. *ScientificWorldJournal*, 2013: 632972.

https://doi.org/10.1155/2013/632972

100. Baldwin J, Antille M, Bonda U, *et al.*, 2014, *In Vitro* pre-vascularisation of tissue-engineered constructs a co-culture perspective. *Vasc Cell*, 6: 13.

https://doi.org/10.1186/2045-824X-6-13

101. Tufro-McReddie A, Norwood V, Aylor K, *et al.*, 1997, Oxygen regulates vascular endothelial growth factor-mediated vasculogenesis and tubulogenesis. *Dev Biol*, 183: 139–149.

https://doi.org/10.1006/dbio.1997.8513

102. Shweiki D, Itin A, Soffer D, *et al.*, 1992, Vascular endothelial growth factor induced by hypoxia may mediate hypoxia-initiated angiogenesis. *Nature*, 359: 843–845.

https://doi.org/10.1038/359843a0

103. Sikavitsas VI, Temenoff JS, Mikos AG, 2001, biomaterials and bone mechanotransduction. *Biomaterials*, 22: 2581–2593.

https://doi.org/10.1016/s0142-9612(01)00002-3

104. Rubin J, Rubin C, Jacobs CR, 2006, Molecular pathways mediating mechanical signaling in bone. *Gene*, 367: 1–16.

https://doi.org/10.1016/j.gene.2005.10.028

105. Weinbaum S, Cowin S, Zeng Y, 1994, A model for the excitation of osteocytes by mechanical loading-induced bone fluid shear stresses. *J Biomech*, 27: 339–360.

https://doi.org/10.1016/0021-9290(94)90010-8

106. Yeatts AB, Fisher JP, 2011, Bone tissue engineering bioreactors: Dynamic culture and the influence of shear Stress. *Bone*, 48: 171–181.

https://doi.org/10.1016/j.bone.2010.09.138

107. Bilodeau K, Mantovani D, 2006, Bioreactors for tissue engineering: focus on mechanical constraints. A comparative review. *Tissue Eng*, 12: 2367–2383.

https://doi.org/10.1089/ten.2006.12.2367

108. Bancroft GN, Sikavitsas VI, van den Dolder J, *et al.*, 2002, Fluid flow increases mineralized matrix deposition in 3D perfusion culture of marrow stromal osteoblasts in a dose-dependent manner. *Proc Natl Acad Sci U S A*, 99: 12600–12605.

https://doi.org/10.1073/pnas.202296599

109. Bancroft GN, Sikavitsas VI, Mikos AG, 2003, Design of a flow perfusion bioreactor system for bone tissue-engineering applications. *Tissue Eng*, 9: 549–554.

https://doi.org/10.1089/107632703322066723

110. Loozen LD, Wegman F, Öner FC, *et al.*, 2013, Porous bioprinted constructs in bmp-2 non-viral gene therapy for bone tissue engineering. *J Mater Chem B*, 1: 6619–6626.

https://doi.org/10.1039/C3TB21093F

111. Cunniffe GM, Gonzalez-Fernandez T, Daly A, *et al.*, 2017, Three-dimensional bioprinting of polycaprolactone reinforced gene activated bioinks for bone tissue engineering. *Tissue Eng Part A*, 23: 891–900.

https://doi.org/10.1089/ten.tea.2016.0498

112. Cidonio G, Alcala-Orozco CR, Lim KS, *et al.*, 2019, Osteogenic and angiogenic tissue formation in high fidelity nanocomposite laponite-gelatin bioinks. *Biofabrication*, 11: 035027.

https://doi.org/10.1088/1758-5090/ab19fd

113. Cidonio G, Glinka M, Kim YH, *et al.*, 2020, Nanoclay-based 3D printed scaffolds promote vascular ingrowth *ex vivo* and generate bone mineral tissue *In Vitro* and *In Vivo*. *Biofabrication*, 12: 035010.

https://doi.org/10.1088/1758-5090/ab8753

114. Sun J, Tan H, 2013, Alginate-based biomaterials for regenerative medicine applications. *Materials* (*Basel*), 6: 1285–1309.

https://doi.org/10.3390/ma6041285

115. Araiza-Verduzco F, Rodríguez-Velázquez E, Cruz H, *et al.*, 2020, Photocrosslinked alginate-methacrylate hydrogels with modulable mechanical properties: Effect of the molecular conformation and electron density of the methacrylate reactive group. *Materials* (*Basel*), 13: 534.

https://doi.org/10.3390/ma13030534

116. Wu Y, Hospodiuk M, Peng W, *et al.*, 2018, Porous tissue strands: Avascular building blocks for scalable tissue fabrication. *Biofabrication*, 11: 015009.

https://doi.org/10.1088/1758-5090/aaec22

117. Wehrle M, Koch F, Zimmermann S, *et al.*, 2019, Examination of hydrogels and mesenchymal stem cell sources for bioprinting of artificial osteogenic tissues. *Cell Mol Bioeng*, 12: 583–597.

118. Chiesa I, De Maria C, Lapomarda A, *et al.*, 2020, Endothelial cells support osteogenesis in an *in vitro* vascularized bone model developed by 3D bioprinting. *Biofabrication*, 12: 025013.

https://doi.org/10.1088/1758-5090/ab6a1d

119. Kim H, Yang GH, Choi CH, *et al.*, 2018, Gelatin/PVA scaffolds fabricated using a 3d-printing process employed with a low-temperature plate for hard tissue regeneration: fabrication and characterizations. *Int J Biol Macromol*, 120: 119–127.

https://doi.org/10.1016/j.ijbiomac.2018.07.159

120. Wang X, Tolba E, Schröder HC, *et al.*, 2014, Effect of bioglass on growth and biomineralization of saos-2 cells in hydrogel

after 3D cell bioprinting. *PLoS One*, 9: e112497.

https://doi.org/10.1371/journal.pone.0112497

121. Heo DN, Alioglu MA, Wu Y, *et al.*, 2020, 3D bioprinting of carbohydrazide-modified gelatin into microparticle-suspended oxidized alginate for the fabrication of complex-shaped tissue constructs. *ACS Appl Mater Interfaces*, 12: 20295–20306.

https://doi.org/10.1021/acsami.0c05096

122. Costantini M, Idaszek J, Szöke K, *et al.*, 2016, 3D bioprinting of bm-mscs-loaded ecm biomimetic hydrogels for *in vitro* neocartilage formation. *Biofabrication*, 8: 035002.

https://doi.org/10.1088/1758-5090/8/3/035002

123. Liu B, Li J, Lei X, *et al.*, 2020, 3D-bioprinted functional and biomimetic hydrogel scaffolds incorporated with nanosilicates to promote bone healing in rat calvarial defect model. *Mater Sci Eng C Mater Biol Appl*, 112: 110905.

https://doi.org/10.1016/j.msec.2020.110905

124. Chimene D, Miller L, Cross LM, *et al.*, 2020, Nanoengineered osteoinductive bioink for 3D bioprinting bone tissue. *ACS Appl Mater Interfaces*, 12: 15976–15988.

https://doi.org/10.1021/acsami.9b19037

125. Sun X, Ma Z, Zhao X, *et al.*, 2021, Three-dimensional bioprinting of multicell-laden scaffolds containing bone morphogenic protein-4 for promoting m2 macrophage polarization and accelerating bone defect repair in diabetes mellitus. *Bioact Mater*, 6: 757–769.

https://doi.org/10.1016/j.bioactmat.2020.08.030

126. Dubey N, Ferreira JA, Malda J, *et al.*, 2020, Extracellular matrix/amorphous magnesium phosphate bioink for 3d bioprinting of craniomaxillofacial bone tissue. *ACS Appl Mater Interfaces*, 12: 23752–23763.

https://doi.org/10.1021/acsami.0c05311

127. Sawkins MJ, Mistry P, Brown BN, *et al.*, 2015, Cell and protein compatible 3d bioprinting of mechanically strong constructs for bone repair. *Biofabrication*, 7: 035004.

https://doi.org/10.1088/1758-5090/7/3/035004

128. Ahlfeld T, Doberenz F, Kilian D, *et al.*, 2018, Bioprinting of mineralized constructs utilizing multichannel plotting of a self-setting calcium phosphate cement and a cell-laden Bioink. *Biofabrication*, 10: 045002.

https://doi.org/10.1088/1758-5090/aad36d

129. Zhai X, Ruan C, Ma Y, *et al.*, 2018, 3D-bioprinted osteoblast-laden nanocomposite hydrogel constructs with induced microenvironments promote cell viability, differentiation, and osteogenesis both *In Vitro* and *In Vivo*. *Adv Sci* (*Weinh*), 5: 1700550.

https://doi.org/10.1002/advs.201700550

130. Campos DF, Blaeser A, Buellesbach K, *et al.*, 2016, Bioprinting organotypic hydrogels with improved mesenchymal stem cell remodeling and mineralization properties for bone tissue engineering. *Adv Healthc Mater*, 5: 1336–1345.

https://doi.org/10.1002/adhm.201501033

131. Anada T, Pan CC, Stahl AM, *et al.*, 2019, Vascularized bone-mimetic hydrogel constructs by 3D bioprinting to promote osteogenesis and angiogenesis. *Int J Mol Sci*, 20: 1096.

https://doi.org/10.3390/ijms20051096

132. Bernal PN, Delrot P, Loterie D, *et al.*, 2019, Volumetric bioprinting of complex living-tissue constructs within seconds. *Adv Mater*, 31: 1904209.

133. Heo DN, Ayan B, Dey M, *et al.*, 2020, Aspiration-assisted bioprinting of co-cultured osteogenic spheroids for bone tissue engineering. *Biofabrication*, 13: 015013.

https://doi.org/10.1088/1758-5090/abc1bf

134. Rukavina P, Koch F, Wehrle M, *et al.*, 2020, *In Vivo* evaluation of bioprinted prevascularized bone tissue. *Biotechnol Bioeng*, 117: 3902-11.

https://doi.org/10.1002/bit.27527

135. Ashammakhi N, Ahadian S, Xu C, *et al.*, 2019, Bioinks and bioprinting technologies to make heterogeneous and biomimetic tissue constructs. *Mater Today Bio*, 1: 100008.

https://doi.org/10.1016/j.mtbio.2019.100008

136. Mercado-Pagán ÁE, Stahl AM, Shanjani Y, *et al.*, 2015, Vascularization in bone tissue engineering constructs. *Ann Biomed Eng*, 43: 718–729.

https://doi.org/10.1007/s10439-015-1253-3

137. Ramtani S, 2008, Electro-mechanics of bone remodelling. *Int J Eng Sci*, 46: 1173–1182.

https://doi.org/10.1016/j.ijengsci.2008.06.001

138. Moura D, Pereira RF, Gonçalves IC, 2022, Recent advances on bioprinting of hydrogels containing carbon materials. *Mater Today Chem*, 23: 100617.

https://doi.org/10.1016/j.mtchem.2021.100617